








Cite this: *Environ. Sci.: Atmos.*, 2021, 1, 64

Effect of aromatic ring substituents on the ability of catechol to produce brown carbon in iron(III)-catalyzed reactions†

Henry Chin, ^a Katherine S. Hopstock, ^a Lauren T. Fleming, ^a
Sergey A. Nizkorodov ^{*a} and Hind A. Al-Abadleh ^b

Our previous work demonstrated formation of highly insoluble and strongly light-absorbing organic particles in reactions between catechol or guaiacol with Fe(III) under pH = 3 conditions characteristic of aerosol liquid water. This work extends these measurements to reactions of Fe(III) with 2,4-dinitrophenol, 4-nitrocatechol, 4-methylcatechol, 1,2,4-benzenetriol, 1,2,3-benzenetriol (pyrogallol) and coniferaldehyde to better understand the mechanism of particle formation catalyzed by Fe(III). Particles were observed after 2 h of reactions of catechol (43 ± 1% mass yield), 1,2,4-benzenetriol (32 ± 3%), pyrogallol (27 ± 2%) and coniferaldehyde (35 ± 4%), while reactions of 2,4-dinitrophenol and 4-nitrocatechol did not produce any insoluble products. No particles were observed in reaction of 4-methylcatechol after 2 h, however, insoluble products appeared after a 24 h reaction time. Irradiation of a catechol + Fe(III) mixture by 405 nm light was found to reduce (but not fully suppress) the particle yield due to a competition between photodegradation and Fe(III)-catalyzed oligomerization. Particles produced from precursors + Fe(III) solutions were dissolved in organic solvents and analyzed with ultra performance liquid chromatography coupled to a photodiode array spectrophotometer and a high resolution mass spectrometer. Major separated chromophores were identified as dimeric, trimeric, and tetrameric products of precursor molecules. Purpurogallin was identified as a major reaction product of pyrogallol reaction with Fe(III). To test whether this chemistry can occur in more realistic atmospheric aerosols, reactions of biomass burning organic aerosol (BBOA) extracts with Fe(III) were also examined. Two BBOA samples collected under flaming conditions produced no particles, whereas a BBOA sample produced under smoldering conditions resulted in particle formation under both dark and 405 nm irradiation conditions. The results suggest that Fe(III)-catalyzed chemistry can take place in aging BBOA plumes resulting from smoldering fires and make aerosol particles more light-absorbing.

Received 24th September 2020
Accepted 24th November 2020

DOI: 10.1039/d0ea00007h

rsc.li/esatmospheres

Environmental significance

Mineral dust particles and biomass burning smoke frequently occur in the same atmospheric environment. Our previous work demonstrated formation of highly insoluble and strongly light-absorbing organic particles in reactions between catechol or guaiacol, typical biomass burning compounds, with Fe(III), which is common in mineral dust. This work extends these measurements to reactions of Fe(III) with 2,4-dinitrophenol, 4-nitrocatechol, 4-methylcatechol, 1,2,4-benzenetriol, 1,2,3-benzenetriol (pyrogallol) and coniferaldehyde to better understand the mechanism of particle formation catalyzed by Fe(III). We were able to observe particle formation in reactions of catechol, 1,2,4-benzenetriol, pyrogallol and coniferaldehyde, but not in reactions of 2,4-dinitrophenol, 4-nitrocatechol and 4-methylcatechol. These reactions were not suppressed by UV radiation, suggesting that they can happen during both night and day. To test whether this chemistry can occur in more realistic atmospheric aerosols, reactions of a limited number of biomass burning organic aerosol extracts with Fe(III) were also examined. Two BBOA samples collected under flaming conditions produced no particles, whereas a BBOA sample produced under smoldering conditions resulted in particle formation. The results suggest that Fe(III)-catalyzed chemistry can take place in aging BBOA plumes resulting from smoldering fires and make aerosol particles more light-absorbing. Particles that are darker in color are expected to have stronger direct effect on climate by absorbing solar radiation.

^aDepartment of Chemistry, University of California, Irvine, California 92697, USA.
E-mail: nizkorod@uci.edu

^bDepartment of Chemistry and Biochemistry, Wilfrid Laurier University, Waterloo, ON, N2L 3C5, Canada

† Electronic supplementary information (ESI) available: Scheme of oxidation of guaiacol by Fe(III), UPLC-PDA-HRMS data for the 3-HC and 4-HC reactions with Fe(III), and results of suppression of particle yield by 405 nm radiation in catechol + Fe(III) reaction. See DOI: 10.1039/d0ea00007h

1. Introduction

Organic compounds represent a major fraction of atmospheric aerosols particles. While some of these compounds result from primary emissions, others are produced by secondary reactions of various volatile organic compounds (VOCs).¹ The most common mechanism that transforms VOCs into secondary



organic aerosol (SOA) is free-radical driven photooxidation. However, alternative mechanisms also exist. For example, it has been shown that Fe(III) can catalyze oligomerization of certain VOCs leading to much less volatile products. In a study by Slikboer *et al.* (2015), catechol and guaiacol were mixed with Fe(III) at pH 3 at millimolar concentrations, which yielded highly-absorbing, water-insoluble particles of polycatechol and polyguaiacol.² Dissolved iron from acid processing of hematite was also shown to react with catechol and guaiacol under the same conditions to make light-absorbing particles. A follow up study by Al Nimer *et al.* (2019) showed that these oligomerization reactions are not suppressed in the presence of equimolar amounts of oxalate and sulfate ions, which are commonly found in aerosol particles and compete for complex formation with Fe(III).³ Lavi *et al.* (2017) characterized the light-absorbing oligomers formed in Fe(III) reactions with guaiacol, catechol, syringol, *o*- and *p*-cresol, and observed a mixture of strongly-absorbing dimers, trimers, tetramers, and pentamers by liquid chromatography coupled to high resolution mass spectrometry.⁴ Ling *et al.* (2020) demonstrated that Fe-containing clay minerals produced colored particles when exposed to guaiacol.⁵ Pang *et al.* (2019) found strong effect of UV irradiation on chemistry in the Fe(III)-oxalate-guaiacol aqueous mixtures.⁶ These results suggest that aqueous reactions of phenolic compounds with Fe(III) may serve as an efficient source of light-absorbing organic compounds in atmospheric particles, which are collectively known as “brown carbon”.^{7,8}

Dihydroxybenzenes catechol, resorcinol, and hydroquinone are major constituents of biomass burning organic aerosol (BBOA).^{9,10} Since biomass burning is one of the largest emission sources of organics, these compounds are ubiquitous in the atmosphere. Of these three, catechol forms the strongest complex with Fe(III) because its adjacent phenolic groups make it an excellent bidentate ligand, and reactions of this complex then lead to the light-absorbing products. Likewise, aerosol particles containing Fe(III) are also widespread in the atmosphere.¹¹ The dominant type of Fe-containing particles is mineral dust¹² because iron is the most abundant transition metal in the Earth's crust.¹³ Other sources of Fe in the atmosphere include anthropogenic combustion from coal burning,^{14,15} biomass burning,^{16,17} and brake wear.¹⁸ There are realistic scenarios in which catechol and related compounds can end up in iron-containing particles. For example, primary particles from cooking emissions contain internally mixed soluble iron and organics.¹⁹ Smoke from biomass burning is often spread by wind, which also lifts crustal particles off the ground. Mineral dust is known to be transported globally by wind,^{20,21} and BBOA similarly travels long distances,²² offering ample time for partitioning of organic vapors into Fe-containing particles.

In addition to catechol, BBOA also contains many other related compounds that can potentially react with Fe(III) by similar mechanisms, however, their reactivity towards Fe(III) is yet to be investigated. A study by Salgado *et al.* suggested that compounds similar to catechol such as 4-*tert*-butylcatechol and 3,4-dihydroxybenzaldehyde behave differently after mixing the organic solution with ferric nitrate as the result of electron

affinity of their respective functional group.²³ Their computational work led to a proposed mechanism of oxidation of substituted catechols by Fe(III) with three major steps. The first one is complex formation between iron and the dihydroxybenzenes, followed by inner-sphere ligand to iron charge transfer, and then deprotonation of one of the oxygen atoms leading to quinone formation. Other compounds found in BBOA include guaiacol and its derivatives. The reaction mechanism of these compounds with Fe(III) is believed to be similar to that with Mn(III) reported by Hwang *et al.* (2008).²⁴ In this mechanism, Mn(III) abstracts an electron from the -OH substituent forming a phenoxy radical stabilized by resonance. Then, C-C coupling reactions of radicals and additional electron abstractions by Mn(III) lead to the formation of dimers and trimers, and eventually polyguaiacol.²⁵

In this study, we further explore several catechol derivatives to better understand the mechanism of particle formation catalyzed by Fe(III). Reaction of catechol (CA) with Fe(III) is used as a reference system to ensure that the previous results are reproducible. Reaction of 2,4-dinitrophenol (DNP) with Fe(III) is tested to verify the necessity of having two adjacent phenolic groups for the initial metal complexation to occur. To examine the effect of the type and location of catechol ring substituents, reactions of 4-nitrocatechol (NC), 4-methylcatechol (MC), 1,2,4-benzenetriol (4-HC), and pyrogallol (3-HC) are compared. In addition, the reaction of Fe(III) with coniferaldehyde (CON) is tested to compare its reactivity to that of the structurally similar guaiacol. All of the compounds selected for these experiments are commonly found in BBOA. To check whether this chemistry can occur in more realistic atmospheric samples, reactions of BBOA extracts with Fe(III) are also examined. Finally, the effect of near-UV radiation on this chemistry is also examined. The overarching conclusion of this study is that the amount and color of insoluble particles depends in a complicated way on the type of the organic reactant and, in the case of BBOA, the conditions under which the fuel is burned.

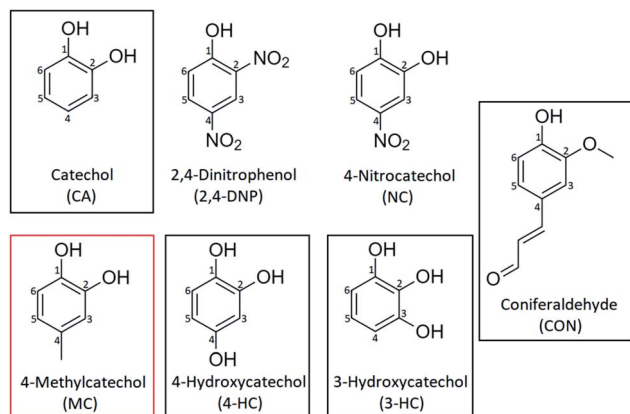
2. Experimental

2.1 Chemicals and solution preparation

The structures of organic compounds used in this work are shown in Scheme 1. All chemicals were used as received without further purification: catechol (1,2-benzenediol, >99%, CAS 120-80-9, Acros Organics), 4-nitrocatechol (4-nitrobenzene-1,2-diol, 97%, CAS 3316-09-4, Acros Organics), coniferaldehyde (4-hydroxy-3-methoxycinnamaldehyde, 98%, CAS 458-36-6, Sigma-Aldrich), 4-methylcatechol (4-methylbenzene-1,2-diol, >95%, CAS 452-86-8, Sigma-Aldrich), pyrogallol (1,2,3-benzenetriol, 99%, CAS 87-66-1, Alfa Aesar), 1,2,4-benzenetriol (97%, 533-73-3, Alfa Aesar), and iron(III) chloride hexahydrate (97%, CAS 10025-77-1, Sigma-Aldrich).

All solutions were freshly prepared for each experiment by dissolving the chemical in 10 mM stock solution of KCl (CAS 7447-40-7, EM Science) in nanopure water, with KCl added in order to stabilize pH reading. The pH was adjusted using concentrated hydrochloric acid (37.5%, CAS 7647-01-0, Fisher Scientific) and verified with a calibrated Mettler Toledo





Scheme 1 Chemical structures and abbreviation codes of pyrocatechol (CA), 2,4-dinitrophenol (2,4-DNP), 4-nitrocatechol (NC), coniferaldehyde (CON), 4-methylcatechol (MC), 4-hydroxycatechol (4-HC), and 3-hydroxycatechol (3-HC). The frames in black highlight the organic compounds that produced particles promptly due to reaction with Fe(III); MC is surrounded by a red frame because it produced particles on a slower time scale.

SevenEasy S20 pH meter. Because the formation of the bidentate mononuclear complex is pH sensitive,^{26,27} the initial pH values were adjusted to 3, a common pH in aerosol particles.²⁸ As the pH becomes higher (>4), catechol and its analogs start to lose protons on hydroxyl groups and form complexes with higher coordination numbers. A similar phenomenon can be found in hydrolytic Fe(III) species as well.²⁹

2.2 UV-Vis experiments under dark conditions

The 10 mM KCl stock solution at pH 3 was used to prepare 10 mL of 80 mM iron(III) chloride, FeCl₃, and 100 mL of 1.06 mM catechol derivative. After the preparation, the catechol derivative solution was then re-adjusted to pH 3. A 0.5 mL volume of 80 mM of FeCl₃ was mixed with 19 mL of 1.06 mM of a catechol derivative in a 20 mL scintillation vial resulting in an iron to organic molar ratio of 2 mM : 1 mM. These relatively high concentrations were selected to mimic aqueous surfaces where organic compounds are enriched. The concentrations used were the same in all experiments as we focused on the effect of the catechol derivative on the particle yield. A typical concentration of dissolved Fe(III) in cloud droplets (diameter ~20 μm) is around 10⁻⁶ M.³⁰ Therefore, for an aerosol particle produced by evaporation of cloud droplets down to a diameter of 1 μm, the concentration of dissolved Fe(III) could be as high as 10 mM, making the 2 mM Fe(III) concentration in our experiments a relevant choice for aerosol particles. The gas-phase concentration of catechol can be as high as 50 ppbv (~5 × 10⁻⁸ atm) resulting from biomass burning, pyrolysis and combustion,³¹ but in most cases it will be well below 1 ppbv (10⁻⁹ atm) level. With the Henry's law constant of 4600 M atm⁻¹,³² this translates into 0.2 mM and 0.005 mM, respectively, in a bulk system like a cloud droplet. The concentrations could be higher in the interfacial region of the particles because of surface enhancement of organics. In our experiments, we selected 1 mM

concentration of catechol to ensure that Fe is in excess but at the same time a measurable amount of products can be produced on a reasonable experimental time scale of 2 h.

The mixture was covered by Al foil to avoid photochemistry. The mixture was stirred on a stir plate at room temperature. The vial was closed but not sealed allowing the room air to interact with the solution during this process. UV-Vis spectra of the mixture were collected by withdrawing 0.5 mL of the mixture out of the vial, diluting 8-fold using nanopure water in a 1 cm quartz cuvette at 1–5 min, 1 h, and 2 h time points using Shimadzu UV-2450 spectrophotometer with the reference cuvette containing 3 mL of nanopure water. Shortly after the 2 h time point, the solution was filtered *via* a pre-weighed nylon membrane (0.20 micron pore size, 25 mm diameter, EMD) by syringe filtration, and a UV-Vis spectrum of the filtrate was also collected. The filter was dried for 24 h, and weighted to estimate the particle yield. Filter weighing was done with Sartorius ME5-F microbalance (1 μg precision). More precise particle yield measurements were done with larger amounts of reagents, as described below.

2.3 Mass yield experiments

For these experiments, the starting amounts of both reactants were scaled up compared to the amounts used in Section 2.2. The 10 mM KCl stock solution at pH 3 was used to prepare 10 mL of 20 mM FeCl₃ and 100 mL of 1 mM catechol derivative. The pH was re-adjusted to 3. To initiate the reaction, the two solutions were mixed in a 250 mL beaker to achieve the iron to organic ratio of 2 : 1, and the mixture was covered by Al-foil. After 2 h of mixing on a stir plate, the mixture was filtered through a pre-weighed nylon membrane (0.20 micron pore size, 47 mm diameter, EMD) by syringe filtration. The filtration was performed one more time through the same filter, and the filter was washed with 50 mL of nanopure water to remove residual soluble salts. The filter was dried for 24 hours, weighed, and the effective product mass yield was calculated using the following formula (eqn (1)):

$$\text{Yield}(\%) = \frac{\text{mass}_{\text{dried filter}} - \text{mass}_{\text{original filter}}}{\text{mass}_{\text{organic reactant}}} \times 100\% \quad (1)$$

2.4 Dynamic Light Scattering experiments

Dynamic Light Scattering (DLS) experiments were performed using Malvern Zetasizer Nano DLS. Solutions of 10 mL of 80 mM FeCl₃ and 100 mL of 1.06 mM of a catechol derivative were prepared and adjusted to pH 3 as described above. A volume of 0.5 mL of 80 mM of FeCl₃ was mixed with 19 mL of 1.06 mM of a catechol derivative, and 3 mL of this mixture was transferred immediately to a cuvette for the measurement. The dispersant was water; backscattering angle was -173° by default; viscosity was set to 0.0082 cP; the equilibrium temperature was 25 °C; the real refractive index of the material was set to 1.604 and the imaginary refractive index was set to 0.000 (the exact values do not affect the results presented below). Each measurement had 6 runs and a 120 second waiting time, and each run lasted 10



seconds. Ten measurements were taken for each DLS experiment. Both derived count rate (kcps) and Z-average diameter (nm) were collected and plotted against the time of reaction (which lasted 30 min in these experiments). The error bars were calculated based on two sets of data using the first standard deviation (σ).

2.5 Analysis of reactions products

Black particles from reactions of 3-HC, 4-HC, and CON were analyzed with Thermo Scientific Vanquish Horizon ultra performance liquid chromatograph coupled to a Vanquish Horizon photodiode array spectrophotometer and to a Q Exactive Plus high resolution mass spectrometer with a resolving power up to 1.4×10^5 (UPLC-PDA-HRMS). The dried filters remaining from the mass yield experiments described in Section 2.3 were cut into 8 segments, and one segment was extracted in 20 mL methanol using a vortex shaker. After 30–45 min of shaking, the filters were removed. The extraction solutions were colored and filters were lighter in color but not completely white indicating that only some reaction products could be dissolved by this method (particles from the CA + Fe(III) reaction could not be dissolved in methanol or other common organic solvents). The solutions were evaporated on a rotary evaporator, and the residues were re-dissolved in a 20 mL mixture of acetonitrile and water (50% each by volume) and filtered through a syringe filter. The column was Phenomenex Luna Omega Polar C18, 150×2.1 mm, with $1.6 \mu\text{m}$ particles and 100 \AA pores, maintained at $30 \text{ }^\circ\text{C}$ during the runs, and the injected volume was kept at $5 \mu\text{L}$. The eluent flow of 0.3 mL min^{-1} consisted of a mixture of water acidified with 0.1% formic acid to pH 3 (solution A) and acetonitrile with a 0.1% formic acid added (solution B). The gradient was: 0–3 min 95% A; 3–14 min linear ramp to 95% B; 14–16 min hold at 95% B; 16 min return to 95% A and hold until 22 min in preparation for the next run. PDA collected data at 5 Hz over 190–580 nm range with a 4 nm effective bandwidth. Mass spectra were obtained with HRMS operating first in positive ion mode, and then in a separate UPLC scan in the negative ion mode. The heated electrospray ionization (HESI) ion source parameters were: +3.5 kV and –3.5 kV spray voltage, $300 \text{ }^\circ\text{C}$ probe heater temperature, $320 \text{ }^\circ\text{C}$ capillary temperature, 50 units of sheath gas flow, and 10 units of aux gas flow. All peaks were analyzed using the Thermo Scientific program FreeStyle 1.6. The strongest peaks contributing to the near-UV and visible PDA chromatogram were correlated to the corresponding peaks in the total ion current (TIC) chromatogram, taking into account a delay time of 0.06 min between the PDA and Orbitrap detectors. The suspect TIC peaks were confirmed by examining selected ion monitoring (SIM) chromatograms. Ion formulas generated by FreeStyle were verified with a molecular formula calculator (<https://fs.magnet.fsu.edu/~midas/>). In addition to running samples, standard solutions of CA, 3-HC, coniferaldehyde, and 4-HC were run on UPLC-PDA-HRMS to verify that no oxidation of standards occurred in the HESI source (such oxidation of CA was observed in our previous work with a different ESI instrument and complicated assignments).² CA, 3-HC and CON standards

gave clean single-peak chromatograms with no major impurities or oxidation products. 4-HC standard results showed that the starting material was contaminated and, as a result, a few autooxidation products were present, however, 4-HC was still the main component of the standard.

2.6 BBOA UV-Vis experiment

Dried pine needles were burned and the resulting biomass burning organic aerosol (BBOA) particles were sampled during different burning stages on Fluoropore PTFE Membrane Filters (Millipore FGLP04700, $0.20 \mu\text{m}$ pore size, 47 mm diameter) at 10 L min^{-1} . Each filter was extracted in 18 mL of 10 mM KCl solution at pH 3 by shaking the solution for 1 h. Not all BBOA material could be extracted as the filter remained brown after the extraction. Since the solubility of BBOA material is unknown, we used a typical value of mass absorption coefficient (MAC)³³ at 365 nm equal to $\sim 1 \text{ m}^2 \text{ g}^{-1}$ to estimate the mass concentration of BBOA compounds (C_{mass}) in the extract from the measured base 10 absorbance (A) and cuvette path length (l), as shown in the following formula (eqn (2)):

$$\text{MAC}(\lambda) = \frac{A(\lambda) \times \ln(10)}{l \times C_{\text{mass}}} \quad (2)$$

The molar concentration of BBOA compounds in the extract was estimated assuming an average molecular weight of 200 g mol^{-1} . A pH = 3 solution of FeCl_3 in 10 mM KCl was then added to achieve an estimated Fe(III):organics molar ratio of 2 : 1, which produced the maximal particle yield in our previous study of Fe(III) + catechol reaction.² The reaction took place under dark conditions. The solution was exposed to air, allowing O_2 to participate as an oxidant. After a certain reaction time, 1 mL of the solution was filtered through a syringe filter to eliminate suspended particulates, transferred into a cuvette and diluted 4-fold to take a UV-Vis spectrum.

2.7 Effect of near-UV irradiation on particle formation

The procedure was similar to the procedure in Section 2.2. However, the mixture was not covered by Al foil and was instead irradiated from above through the opening in the scintillation vial. The vial was fully open to room air during this process. UV radiation at 405 nm was used because oxidation species of Fe-catechol complex has a strong absorption band at 400 nm. The radiation was produced by a light-emitting diode (LED, M405L4, Thorlabs) with a center wavelength of $405 \pm 7 \text{ nm}$ (the quoted range refers to full width at half maximum). Two different intensities of the UV light were tested: one with the maximal LED output ($\sim 135 \text{ mW}$), and another with LED power set to 50% of the maximal value ($\sim 70 \text{ mW}$).

3. Results and discussion

3.1 Dark reaction between Fe(III) and organic reactants

Fig. 1 (a–g) show the absorption spectra recorded after 1–5 min, 1 h and 2 h of reactions, as well as spectra of solutions after filtering out the particles. It also shows the corresponding



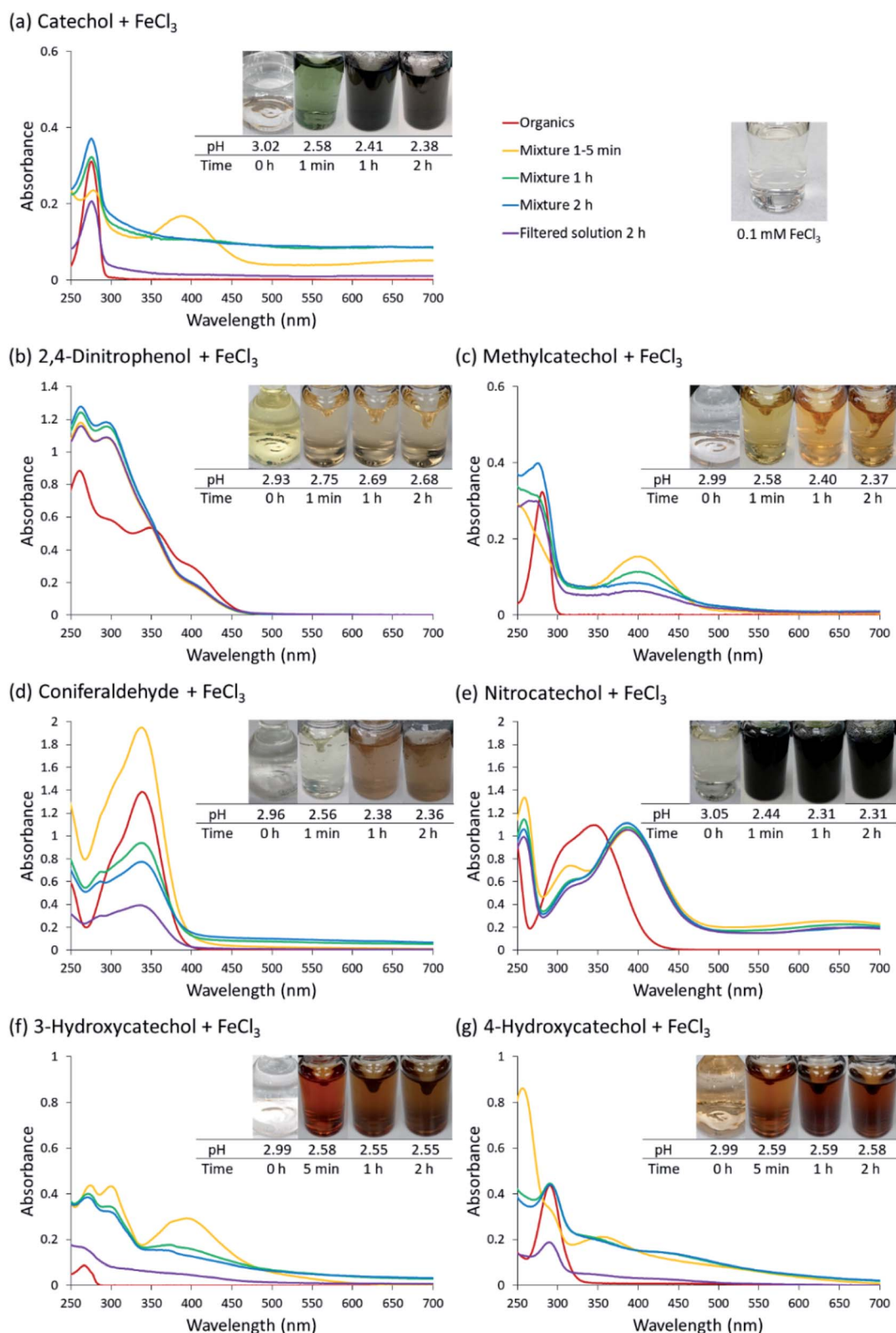


Fig. 1 UV-Vis absorption spectra of mixtures of Fe(III) with (a) pyrocatechol, (b) 2,4-dinitrophenol, (c) 4-methylcatechol, (d) coniferaldehyde, (e) 4-nitrocatechol, (f) 3-hydroxycatechol, and (g) 4-hydroxycatechol. Different colors of traces correspond to spectra of organic reactant before mixing (red), 1–5 min after mixing (orange), 1 h after mixing (green), 2 h after mixing (blue), and filtered solution (purple). The final concentration of organics is 1 mM, and the final concentration of Fe(III) is 2 mM. The photographs are those of unfiltered solutions.



photographs of the reacting mixture vials taken over time. Several species contribute to the overall light absorption in the reaction mixtures of Fe(III) and organic reactants. Prior to mixing, the Fe(III) solution is dominated by the strong absorption band of $\text{Fe}(\text{OH})_2^+$ at 296 nm, and the organic reactant solution features a π to π^* transition peaking between 250 and 300 nm, depending on the compound. For example, the π to π^* transition of the aromatic ring in catechol occurs at 276 nm,³⁴ and a similar peak can be observed across all catechol analogs discussed in this paper (Fig. 1). Mixing the solutions results in a sequence of color changes, accompanied in some cases by particle formation. The additional features are observed in the absorption spectrum during the reaction due to: (a) π to π^* transition centered on the ligand in Fe–organics complex appearing in the near-UV and shifted from the corresponding transition in the isolated ligand; (b) ligand-to-metal charge transfer (LMCT) transition in the bidentate iron–organic complexes appearing in the near-IR; (c) bands from soluble reaction products between Fe(III) and the organics reagents, including n to π^* transition in the *o*-quinone species formed from oxidation of catechol–Fe complexes; (d) scattering and absorption by the insoluble suspended particles with a weak wavelength dependence. As demonstrated by Salgado *et al.*,²³ the Fe-complex charge transfer appear quickly after mixing, whereas absorption features of the reaction products take minutes or even hours to develop. In this study, the reaction was terminated after two hours, and presence of particulate products was verified visually as well as by comparing absorption spectra before and after filtering the solution. We will discuss the behavior of each organic reactant shown in Scheme 1 separately over the time frame of our experiments.

Catechol (CA): reaction with CA was carried out multiple times throughout the study because it served as a reference experiment to which reactions of other organic compounds were compared. CA formed complexes with Fe(III) shortly after mixing. An intense peak at 390 nm indicates n to π^* transition of *o*-quinone, which decreased in intensity in one hour, as observed in our previous study.^{2,3} A broad band at 700 nm corresponds to the LMCT transition in the bidentate mononuclear catechol–iron complex.²³ The mixture was intensely green at the beginning; it slowly turned into pale green, while the black tint became progressively prominent. After 2 h of reaction, an overall decrease in transmittance (manifesting itself as increase in the apparent absorbance) across all wavelengths was observed as a result of scattering and absorption by dark colloidal particles formed by the reaction.

2,4-Dinitrophenol (2,4-DNP): to examine the role of bidentate nature of catechol derivatives in the reaction, 2,4-DNP was tested. This compound has only one phenolic group capable of forming a complex with Fe(III), and two nitro groups, which do not contribute to complexation but strongly affect the electron density distribution in the aromatic ring. The mixture remained pale-yellow in color throughout the experiment; and there was no apparent reaction after mixing. There was one band in the spectrum at 295 nm, and no evidence of the LMCT band (which is expected since LMCT appear in bidentate complexes). No particles could be detected at the end of the experiment. These

results confirm the importance of the formation of bidentate catechol–iron complex for the particle formation.^{2,23} In addition, the electron-withdrawing nature of the nitro groups has a suppressing effect on the reactivity, as discussed below.

4-Methylcatechol (MC): reaction of Fe(III) with MC mixture exhibited similar UV-Vis spectrum to that of CA. An intense peak from n to π^* transition at 400 nm of the quinone species appeared promptly and decreased over time. A LMCT band was expected but not observed. It is worth noting that the mixture turned into light green at the moment of the introduction of Fe(III); then it quickly shifted to bright yellow within seconds, and maintained this color for the rest of the experiment, so it is possible the LMCT band disappeared too quickly for us to detect it. There was a slight increase in a peak at around 500 nm observed during the course of two hours. The lack of overall scattering indicates that the mixture did not produce any light-absorbing particles on this time scale. Interestingly, an experiment carried out under the same protocol did produce some coloration on the filter after 3 and 24 h of mixing. The results also show a slight increase in yield after 24 h of mixing. This result coincides with one reported in a previous study by Larson *et al.*, where Mn(II) was used as the catalytic metal ions.³⁵ We conclude that particles can be eventually formed, however the kinetics are much slower compared to the other organic reactants used in this study.

4-Nitrocatechol (NC): before the addition of Fe(III), the spectrum presented an intense broad band with peaks at 310 and 345 nm, attributed to n to π^* transitions. Upon mixing NC and Fe(III), a different n to π^* band of the NO_2 substituent at 386 nm immediately appeared and persisted throughout the observation time. This peak is red shifted relative to its initial position due the deprotonation of catechol moiety as a result of complexation to iron.²⁷ Similar to what was observed in the spectrum of CA, a broad peak at 660 nm, indicative of LMCT for NC–iron complex, was observed from the beginning to the end. The mixture also had an intense, dark green color, akin to the one the catechol–iron mixture had in the beginning. No particle scattering was observed in the UV-Vis spectrum, indicating that the reaction did not go past the formation of the bidentate complex.

3-Hydroxycatechol (3-HC): the 3-HC and Fe(III) reaction exhibited the most complicated color changes in this series of experiments. The 3-HC solution changed from clear to dark, blue-purple a few seconds after adding FeCl_3 , and then quickly turned into dark, amber-orange, which further changed to bright orange, then faded into brown in the first 10 minutes. The UV-Vis spectra indicated that a quinone species absorbing at 371 nm was produced after 5 min; the peak gradually decreased in the two-hour period. The UV-Vis spectrum also had a contribution from scattering by particles by the end of the observation period.

4-Hydroxycatechol (4-HC): 4-HC and Fe(III) reaction demonstrated a similar trend as 3-HC. A product peak was detected around 360 nm in the first 5 min while the solution changed from amber-orange to a brighter orange shade. Unique to this system, as the reaction progressed, the product peak shifted to the red to 450 nm after 1 h. The mixture maintained brown



Table 1 Summary of UV/vis and particle yield observations. The last column contains the average ($n = 3$) effective mass yield in percent (also shown in Fig. 2)

Compound	$n \rightarrow \pi^*$ transition in the <i>o</i> -quinone product (around 400 nm)	LMCT transition (around 700 nm)	Particle mass yield after 2 h (%)
CA	Yes	Yes	43 ± 1
2,4-DNP	—	—	—
4-MC	Yes	—	—
4-NC	Yes	Yes	—
3-HC	Yes	—	27 ± 2
4-HC	Yes	—	32 ± 3
CON	—	—	35 ± 4

color throughout the process. The UV-Vis spectrum also exhibited scattering by suspended particles towards the end of the experiment.

Coniferaldehyde (CON): the mixture of CON and Fe(III) exhibited large changes in intensity of the $n \rightarrow \pi^*$ peak around 337 nm, with the peak first increasing at the 5 min mark and then decreasing over time. No LMCT band was detected, in agreement with the expectation that CON should not form a strong bidentate complex with Fe(III). The solution color changed from a faint green to light orange in the first hour; the color then became progressively darker into brown in the second hour. The overall effective absorbance increased at all wavelengths due to scattering and absorption by the particles, and a large difference was observed between the spectrum of the unfiltered and filtered solution.

In summary, UV/Vis observation of the evolution of near-UV peaks, LMCT broadband peaks, and particle scattering are indicative of the formation of Fe(III)-complexes, which in some cases is followed by the formation of light-absorbing particles (Table 1). The near-UV peak indicative of a $\pi \rightarrow \pi^*$ transition in the Fe-organics complex occurred in all reactions. The $n \rightarrow \pi^*$ transition in the *o*-quinone product was observed in all cases except for 2,4-DNP and CON. A clear LMCT band was observed for CA and 4-NC. Particle formation after 2 h or reaction was observed in CA, 3-HC, 4-HC, and CON. The explanation for this diverse behavior will be presented in Section 3.4.

3.2 Measured particle mass yields

The catechol derivatives that produced particles after 2 h of reaction, namely CA, CON, 3-HC, and 4-HC, were further investigated by scaling up the amounts of reagents to more accurately determine the mass yields. Fig. 2 reproduces the resulting mass yields from Table 1, as well as shows photographs of particles retained on the filters. As much as 30–40% of the initial mass of the dissolved organic reactants was converted into insoluble particles. Previous measurements on CA-derived particles showed that they contained no iron; we presume the same applies to the CON, 3-HC and 4-HC particles (but we have not explicitly verified that). Further experiments using XRF and ICP-MS would be needed to verify the absence of iron in these particles. The reproducibility of experiments was excellent resulting in small standard deviations of the measurements. All

particles appeared dark in color, ranging from brown for CON, dark brown for 3-HC and 4-HC, and black for CA.

3.3 Time-dependence of particle formation under dark conditions

The formation of polymeric particles was further examined using DLS, similar to previous work.^{2,3,36} Fig. 3 shows the time-dependent particle count rate from the reaction of each organic in Scheme 1 and Fe(III) at pH 3 for the first 30 min. The particle count in both NC and MC remained low throughout the experiment, confirming the absence of the particulate reaction products. As discussed below, the electron withdrawing group on NC inhibits the reduction of Fe(III) in the ligand to metal charge transfer step during the catalytic cycle.^{4,23} In the case of MC, which introduces an electron donating group to the 1,2-dihydroxybenzene ring, the particles still form but the kinetics of particle formation is significantly reduced. In contrast, mixtures of CA, 3-HC, 4-HC, and CON with Fe(III) show steady growth in particle count over time, in agreement with large particle yields

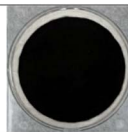


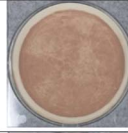

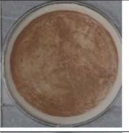




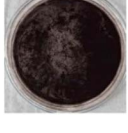

	Trial #1	Trial #2	Trial #3	Yield (%)
CA				43±1%
CON				35±4%
4-HC				32±3%
3-HC				27±2%

Fig. 2 Photographs of filters containing particles after 2 h or reaction, filtration, and drying for catechol (CA), coniferaldehyde (CON), 4-hydroxycatechol (4-HC), and 3-hydroxycatechol (3-HC). The last column contains the average ($n = 3$) effective mass yield in percent.



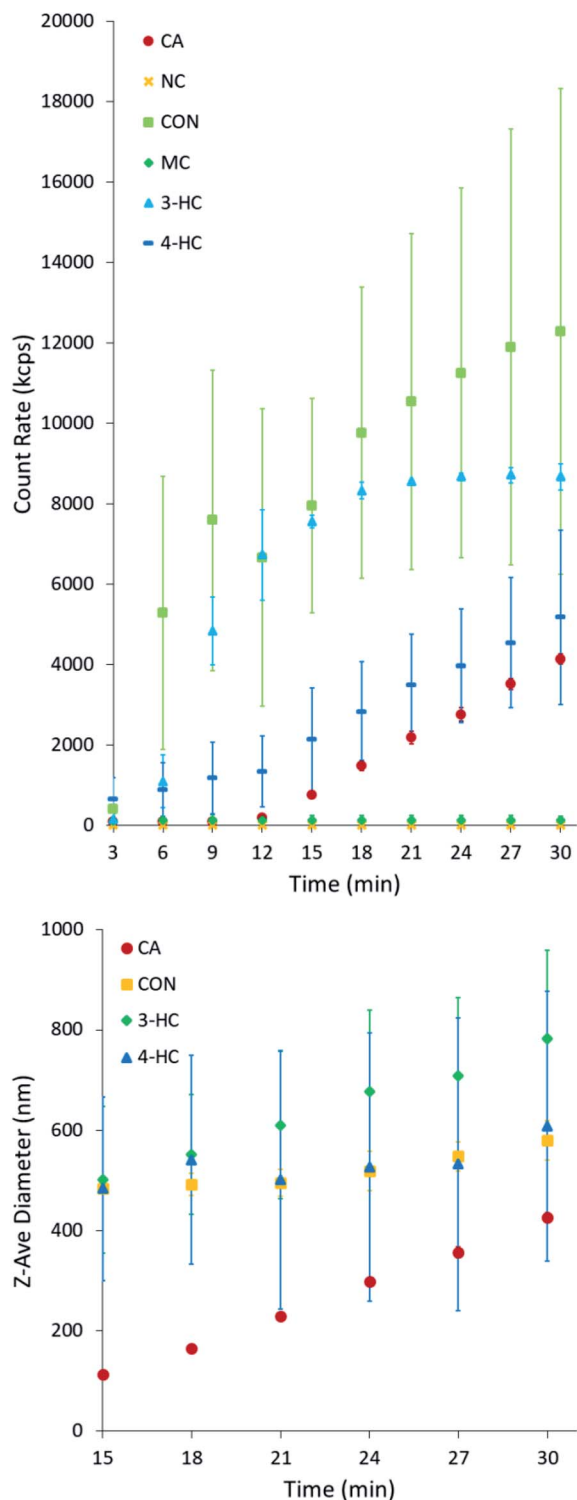


Fig. 3 DLS measurements of the derived count rate of each iron-organic solution mixture as a function of reaction time during the dark conditions. Error bars represent a standard deviation from two repeat measurements.

from these compounds discussed in Section 3.2. CON has the fastest particle growth from the beginning of the experiment as a result of an electron donating group which facilitates the reduction step of the catalytic cycle. We note that the yield from

CON ($35 \pm 4\%$) is actually smaller than that for guaiacol ($49 \pm 14\%$) reported in our previous study,² possibly as a result of steric effects associated with the bulkier substituent group in CON.

3.4 Effect of the substituent groups on the reaction mechanism

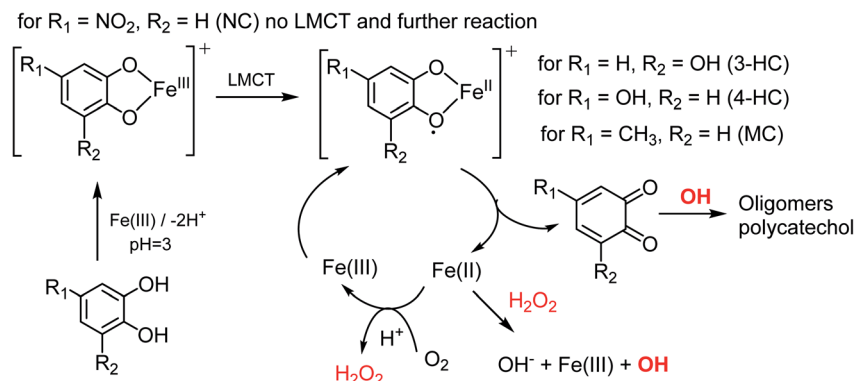
The results described above can be rationalized in terms of the effect of different ring substituents for the catechol and guaiacol derivatives examined here (2,4-DNP is excluded from this comparison because it can only form monodentate complexes with Fe(III)).³⁷

Scheme 2 shows reaction steps involved in the oxidation of catechol as reported earlier.^{23,25,35,38,39} The first step is a formation of an Fe(III)-ligand bidentate complex. This is followed by a ligand to metal charge transfer (LMCT) to Fe(II) complex, and a release of the corresponding 1,2-benzoquinone compound. In presence of oxygen, Fe(II) is oxidized back to Fe(III) producing hydrogen peroxide. The latter serves as a source of OH that drives the oligomerization and other reactions of the 1,2-benzoquinone compound.

The strong electron withdrawing NO₂ group on NC inhibits the LMCT following the formation of a stable NC-Fe(III) complex. Hence, NC showed no detectable yield of particles from the oxidative polymerization reaction steps that follow complexation. In comparison, the hydroxyl substituent in 3-HC and 4-HC can donate the electron to the π -system and help stabilize the LMCT intermediate. Both 3-HC and 4-HC exhibited similar results in reaction with Fe(III), where both compounds formed colored particles with mass yield of $27 \pm 2\%$ and $32 \pm 3\%$ for 3-HC and 4-HC, respectively. MC was also tested to see the effect of a weak electron donating group on the iron-catalyzed polymerization reaction. The mixture of MC and FeCl₃ did not produce particles over the 2 h reaction time. The signature green color of the complex disappeared in seconds after the two solutions were mixed. Meanwhile, a gradual emergence of the peak at 500 nm implies a formation of new, more conjugated product. As mentioned above, particles did eventually appear on the filter after letting the mixture further react for 24 h. The solution after filtration was also visibly lighter in color than the unfiltered solution. DLS measurements also support kinetically slow and inefficient nature of the polymerization of MC by Fe(III).

The reactivity of CON with Fe(III) leading to particle formation is explained by the effective electron donating group, $-\text{CH}=\text{CH}-\text{CHO}$, in the *para* position. As shown in Scheme S1† for guaiacol (no substituents), Fe(III) will abstract an electron from the phenolic group leading to the formation of phenoxy radicals. These radicals are stabilized by resonance and lead to the formation of quinones, dimers and eventually polyguaiacol through C-C coupling reactions. The substituent in CON limits the number of phenoxy radicals available for oxidation and polymerization. Hence, CON is able to rapidly complete the reaction along the pathways that lead to dimer formation. Since *ortho* and *para* position are blocked, formation of higher degree oligomers would be less likely than for guaiacol (Scheme 3). It is





Scheme 2 Suggested mechanisms for the oxidation of catechol derivatives in the presence of excess iron under dark conditions leading to the formation of oligomers and polycatechol particles. The rate of the ligand to metal charge transfer (LMCT) depends on the substituents R_1 and R_2 . The reactions are based on the results from ref. 23, 25, 35, 38 and 39.

possible that the dimers with the $-(\text{CH})_2\text{CHO}$ substituents would be less soluble than CON, and would precipitate out of solution, hence the relatively lower particle mass yield of $35 \pm 4\%$ compared to $49 \pm 14\%$ reported earlier for polyguaiacol.²

3.5 UPLC-PDA-HRMS analysis of particles produced from Fe(III) reactions with 3-HC, CON, and 4-HC

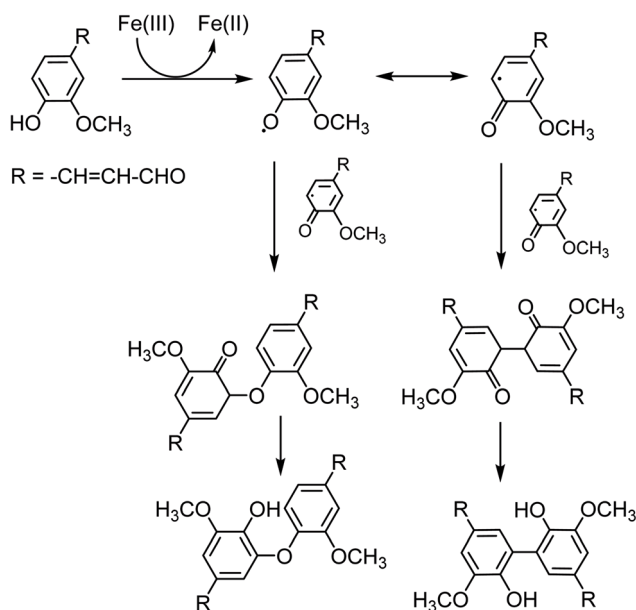
Fig. 4 shows UPLC data for the products of the CON + Fe(III) reaction, which was found to give more detectable products than reactions of 3-HC (Fig. S1[†]) and 4-HC (Fig. S2[†]). Since our focus was on light-absorbing products, we attempted to assign all peaks appearing in the PDA chromatograms at near-UV and visible wavelengths. For all PDA peaks, a suitable companion peak appeared in the TIC chromatograms, and its formula could be confirmed with SIM chromatograms. Table 2

summarizes the retention times (RTs) of major peaks observed in all the PDA chromatograms, and their molecular assignments. The formula of the neutral compounds was obtained by adding a proton to the ion formula assuming that deprotonation was the main ionization mechanism.

In the case of the 3-HC reaction (Fig. S1[†]), only one major absorption peak was detected at RT 9.38 min. Two compounds appeared to co-elute at this RT with neutral formulas of $\text{C}_{24}\text{H}_{14}\text{O}_{10}$ and $\text{C}_{11}\text{H}_8\text{O}_5$. The former has the correct formula for a tetramer of 3-HC. We believe that compound $\text{C}_{11}\text{H}_8\text{O}_5$ corresponds to purpurogallin, which was observed in earlier studies during aerobic oxidation of 3-HC.^{40–43} Purpurogallin has an absorption peak at 325 nm, consistent with the PDA observations. The hydrogen peroxide produced by Fe(II) to Fe(III) oxidation (e.g., Scheme 2) should promote conversion of 3-HC to purpurogallin.

The analysis of the 4-HC products (Fig. S2[†]) was complicated by the initial impurities in the starting 4-HC material. However, the major product at RT 8.18 min has a formula corresponding to an O-bridged dimeric product, $\text{C}_{12}\text{H}_6\text{O}_7$. The low number of H-atoms in this compound suggests a highly-conjugated quinone structure. Another related dimeric product, $\text{C}_{12}\text{H}_6\text{O}_7$, eluted at RT 9.77 min. The rest of the peaks had carbon numbers that were not multiples of 6, suggesting more complicated mechanism than dimerization and other chemistry associated with starting material impurity. We do not have good suggestions for the specific structures of the products beyond the chemical formulas.

The CON + Fe(III) reaction produced a surprisingly large number of peaks (Fig. 4). CON itself $\text{C}_{10}\text{H}_{10}\text{O}_3$ was observed at RT 9.09 min indicating that it was either trapped in particles or produced from particles by decomposition in solution. Several major peaks had 20 carbon atoms in them consistent with dimerization. For example, $\text{C}_{20}\text{H}_{18}\text{O}_6$ eluting as three isomers at 9.79, 10.47 and 10.73 min had the same formula as the two dimers shown in Scheme 3. Three of the compounds had 30 carbon atoms in them, consistent with trimer formation, including $\text{C}_{30}\text{H}_{24}\text{O}_9$, $\text{C}_{30}\text{H}_{26}\text{O}_9$, and $\text{C}_{30}\text{H}_{30}\text{O}_{11}$. Compounds with carbon numbers that were not multiples of 10 were



Scheme 3 Suggested mechanism for the oxidation of CON forming dimers. Compared to the reaction of guaiacol, extensive oligomerization is less likely for CON due to steric constraints.



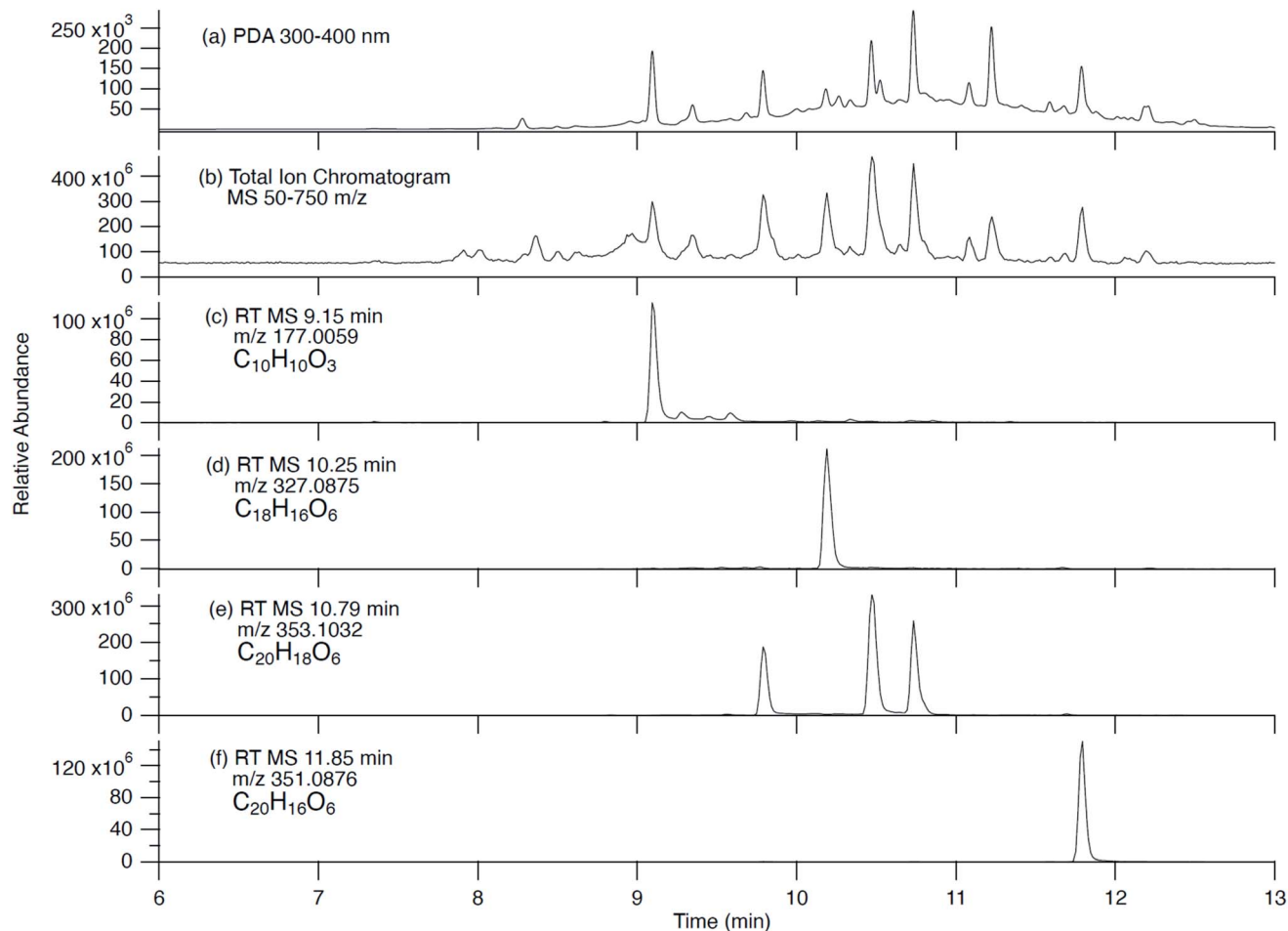


Fig. 4 UPLC-PDA-HRMS data for the CON + Fe(III) reaction products: (a) photodiode array (PDA) chromatogram; (b) total ion current (TIC) chromatogram; and (c & d) single ion monitoring (SIM) chromatograms. The TIC and SIM chromatograms were corrected for the 0.06 min delay time between PDA and Orbitrap detectors. The formulas listed correspond to neutral compounds observed as deprotonated ions at the specified m/z values.

observed as well, such as $C_{18}H_{16}O_6$, and $C_{28}H_{24}O_9$, indicating a loss of two carbon atoms from the CON skeleton before or during oligomerization. At present time, we do not have a good mechanism that explains their formation.

3.6 Reaction of Fe(III) with a mixture of organics in BBOA

Fig. 5 (a–c) show the UV-Vis spectra of the reaction mixture of BBOA and $FeCl_3$ at pH 3 under dark conditions. We found that the results varied depending on the amount of smoldering combustion that occurred while BBOA samples were collected. Sample #1 was taken at the start of the burning when conditions could be characterized as flaming (from the visual inspection of the flame). Upon mixing the extract of sample #1 with $FeCl_3$, the solution color changed from light yellow to a faint yellow of a similar shade. This could be explained simply by mixing of the colors of $FeCl_3$ and dissolved BBOA; there was no strong evidence for a reaction. No further color change was observed afterwards, as shown in the UV-Vis spectrum. There was also no particle yield after the filtration, confirming the absence of reaction. We infer that the BBOA sample #1 either did not contain sufficient quantities of reactive catechol or guaiacol

derivatives or contained compounds with stronger affinity to Fe(III) preventing it from particle-forming reactions. Flaming combustion products include nitrated aromatics, formed from reactions of high levels of NO_x with aromatic vapors,^{44,45} which could have suppressed particle yield.

Sample #2 was collected later in the burning process, when at least half of the fuel burned. Upon mixing with Fe(III), the solution color changed from light yellow to green for about 2 seconds, but then the solution became and remained darker yellow for the next 2 h. The UV-Vis spectrum of the sample #2 mixture showed minimal changes after the first 2 min. The pattern of color change of the mixture of BBOA #2 and $FeCl_3$ was similar to that of the mixture of MC and $FeCl_3$. No particles were detected after syringe filtration at the end of the 2 h reaction time. We infer that BBOA compounds produced during this burning stage may form complexes but they do not partake in the subsequent polymerization over relatively short reaction times, such as, 2 h.

Sample #3 was taken after the fire was extinguished by placing a lid on the container where burning took place. This resulted in purely smoldering conditions, expected to emit



Table 2 Summary of compounds detected by UPLC-PDA-HRMS in negative ion mode from reactions of CON, 4-HC and 3-HC with Fe(III). The formula of the neutral compounds was obtained by adding a proton to the ion formula assuming that deprotonation was the main ionization mechanism

PDA retention time (min)	MS retention time (min)	Description of absorption spectrum observed by PDA	Major <i>m/z</i> values correlating with eluted peak (negative mode)	Relative peak abundance	Neutral formula
From the CON + Fe(III) reaction					
9.09	9.15	222 nm and 338 nm peaks	177.0559	—	C ₁₀ H ₁₀ O ₃
9.35	9.40	200–380 nm broad spectrum	565.1724	—	C ₃₀ H ₃₀ O ₁₁
9.79	9.85	222 nm and 338 nm peaks	353.1032	Major	C ₂₀ H ₁₈ O ₆
			421.0907	Minor	C ₂₃ H ₁₈ O ₈
10.18	10.25	200–400 nm broad spectrum	327.0875	—	C ₁₈ H ₁₆ O ₆
10.47	10.53	222 nm and 342 nm peaks	353.1031	—	C ₂₀ H ₁₈ O ₆
10.73	10.79	222 nm and 338 nm peaks	353.1032	—	C ₂₀ H ₁₈ O ₆
11.08	11.14	222 nm and 338 nm peaks	503.1347	—	C ₂₈ H ₂₄ O ₉
11.22	11.28	222 nm and 338 nm peaks	529.1501	—	C ₃₀ H ₂₆ O ₉
11.79	11.85	200–380 nm broad spectrum	351.0876	—	C ₂₀ H ₁₆ O ₆
12.21	12.25	222 nm and 334 nm peaks	527.1346	—	C ₃₀ H ₂₄ O ₉
From the 4-HC + Fe(III) reaction					
6.28	6.34	210 nm and 318 nm peaks	166.9988	—	C ₇ H ₄ O ₅
6.60	6.66	210 nm peak	237.0042	Major	C ₁₀ H ₆ O ₇
			304.9918	Minor	C ₁₃ H ₆ O ₉
8.18	8.24	218 nm and 336 nm peaks	163.0038	Minor	C ₈ H ₄ O ₄
			261.0039	Major	C ₁₂ H ₆ O ₇
9.77	9.83	218 nm peak	245.0091	—	C ₁₂ H ₆ O ₆
From the 3-HC + Fe(III) reaction					
9.38	9.44	220–340 nm broad spectrum	219.0299	Major	C ₁₁ H ₈ O ₅
			461.0492	Minor	C ₂₄ H ₁₄ O ₁₀

lignin pyrolysis and distillation products.⁴⁶ Upon mixing, the solution color changed from beige-yellow to bright orange. The color then slowly faded and progressively became darker brown over the course of the experiment. Unlike the other two cases discussed above, the UV-Vis spectrum for sample #3 had a notable decrease over time at 480 nm. The pattern of color change of the mixture of BBOA #3 and FeCl₃ matched that of the mixture of 4-HC and FeCl₃. It therefore appears that chemicals produced during the burning at this stage follow the similar mechanism to 4-HC. Syringe filtration of the mixture after 2 hours suggested a large particle mass yield of 53%.

The large differences in the behavior of three different samples of BBOA contrasts with the highly reproducible results of experiments in which individual catechol derivatives were mixed with Fe(III). This suggests that the reaction of aqueous BBOA extracts with Fe(III) is more complex and its outcome may depend strongly upon the specific burning conditions and presumably the nature of the fuel (this was not examined in this study) which dictates BBOA particle composition. We suggest that effect of burning conditions on the reactivity of BBOA towards Fe(III) should be more systematically explored in future studies.

3.7 Reaction in presence of near-UV radiation

Fig. S3† shows the spectra and photographs of solutions of the reaction between Fe(III) and CA collected under 405 nm LED irradiation. A clear trend can be observed from the spectra. As

the LED power increases from 0 mW to 70 mW or 135 mW, the quinone product peak at 390 nm persisted for a longer period of time. In addition, the overall scattering due to suspended particles reduced as the UV intensity increased, and the measured particle yields dropped from 43 ± 2% at 0 mW to 32 ± 6% at 70 mW and 28 ± 2% at 135 mW, as shown in Fig. S4.† The results suggest that photodegradation counteracted the polymerization. Indeed, it was reported that catechol photodegrades under UV irradiation in the presence of O₂.⁴⁷ In an oxidative environment, the easily produced radical caused by irradiation is the main reason for degradation.^{47,48} Nevertheless, the photodegradation was not sufficiently fast to prevent particle formation, suggesting that the chemistry studied here will occur under both dark and sunlit conditions.

4. Atmospheric implications

Experiments described in this paper have broadened the list of organic compounds capable of forming insoluble particles in aqueous reactions with soluble iron. Previous studies found insoluble products in reactions of Fe(III) with catechol, guaiacol, syringol, *o*- and *p*-cresol.^{2,4} We have added 4-hydroxycatechol, 3-hydroxycatechol and coniferaldehyde to the list of particle-forming compounds over short periods of time (*i.e.*, 2 h). In contrast, 2,4-dinitrophenol, 4-nitrocatechol, and 4-methylcatechol did not produce any insoluble products on this time scale. All of these compounds are common constituents of BBOA, but their relative yields depend on the combustion



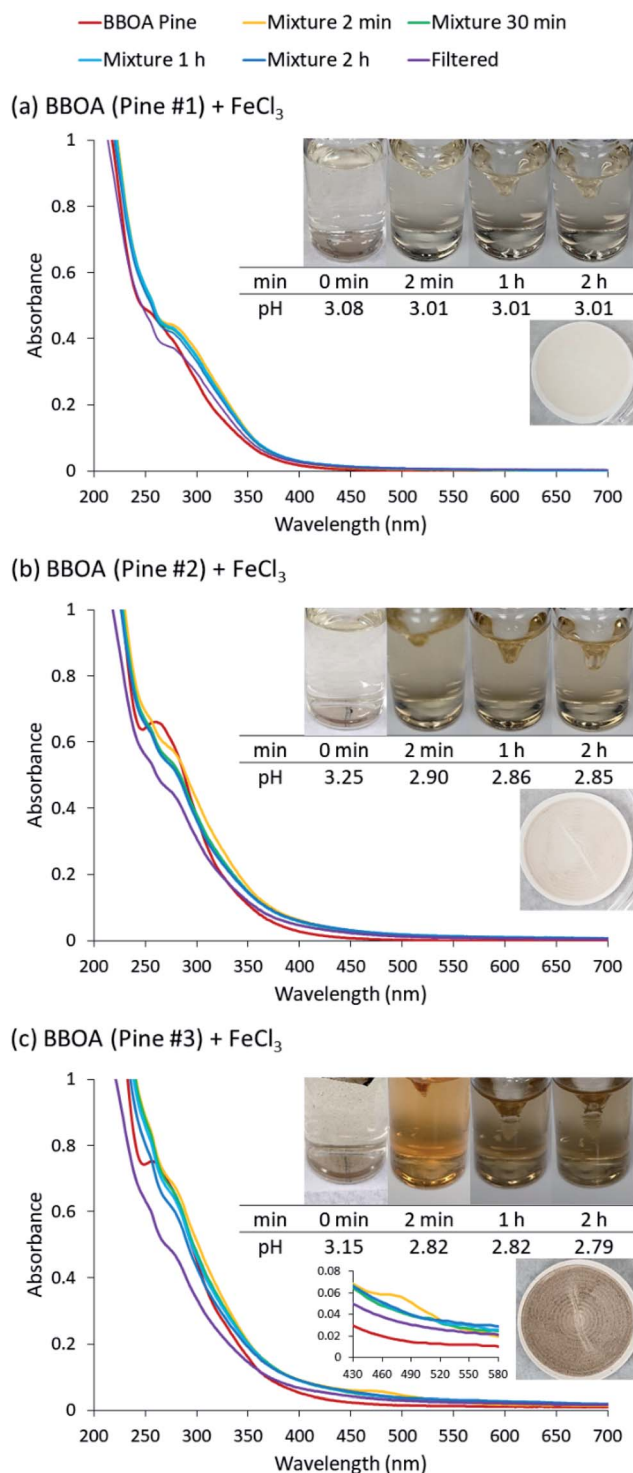


Fig. 5 UV-Vis absorption spectra of mixture of excess Fe(III) and BBOA extracts. Different colors of traces correspond to spectra of BBOA before mixing (red), 2 min after mixing (orange), 30 min after mixing (green), 1 h after mixing (light blue), 2 h after mixing (dark blue), and filtered solution (purple).

conditions. We have been able to directly demonstrate that BBOA produced under smoldering conditions (favoring lignin pyrolysis and distillation products) can produce particles in Fe(III)-catalyzed reactions, whereas BBOA produced under

flaming conditions (favoring nitroaromatics) does not appreciably react in presence of Fe(III). The results suggest that Fe(III)-catalyzed chemistry can take place in smoldering BBOA plumes and make aerosol particles more light-absorbing. This has important implications for understanding the direct effect of BBOA and mixed dust/BBOA aerosols on climate.

The millimolar concentrations of Fe(III) and organic reactants used in our experiments may only be attainable on surfaces of particles or in aerosol liquid water, so the results of this study should not be applied to cloud and fog droplets, where the concentrations are lower. Furthermore, these experiments have not evaluated the possible effect of competing complexation between Fe(III) and oxalate ion, which has been shown to decrease the particle yield in Fe(III) + catechol reaction.³ Finally, in real particles, there are other organic compounds that do not form complexes with Fe(III) but can scavenge OH (an intermediate in this chemistry), thus indirectly affecting the chemistry leading to particle formation. This makes it challenging to extrapolate these results to actual atmospheric conditions.

UV irradiation of aqueous organic aerosol tends to fragment organic compounds producing smaller, more volatile compounds from larger oligomeric ones.^{49–51} Light-absorbing compounds derived from BBOA have also been found to fragment and photobleach under irradiated conditions.⁵² Such photodegradation processes can be amplified in presence of Fe(III), which efficiently catalyzes photo-Fenton processes.^{53–57} We tested whether 405 nm irradiation can suppress Fe(III)-catalyzed oligomerization reactions in the catechol + Fe(III) system. The irradiation was found to reduce, but not fully suppress the particle yield. This important result shows that chemistry described in this study is not limited to nighttime, and can also take place under sunlit conditions.

Author contributions

The experiments and data analysis were conceived by SAN and HAA, and carried out by HC and LTF. KSH did the analysis of UPLC-PDA-HRMS data. All authors have given approval to the final version of the manuscript.

Conflicts of interest

The authors declare no competing financial interest.

Acknowledgements

The authors acknowledge support from US NSF grant AGS-1853639. The UPLC-PDA-HRMS instrument was purchased with NSF grant CHE-1920242. H. A. A. acknowledges funding from NSERC and the Fulbright Canada Research Chair in Atmospheric Chemistry, Air Quality and Climate Change program at the University of California, Irvine. We acknowledge the UCI Laser Spectroscopy Laboratory and its director Dr Dmitry Fishman for help with the DLS measurements.



References

- M. Hallquist, J. C. Wenger, U. Baltensperger, Y. Rudich, D. Simpson, M. Claeys, J. Dommen, N. M. Donahue, C. George, A. H. Goldstein, J. F. Hamilton, H. Herrmann, T. Hoffmann, Y. Iinuma, M. Jang, M. E. Jenkin, J. L. Jimenez, A. Kiendler-Scharr, W. Maenhaut, G. McFiggans, T. F. Mentel, A. Monod, A. S. H. Prevot, J. H. Seinfeld, J. D. Surratt, R. Szmigielski and J. Wildt, The formation, properties and impact of secondary organic aerosol: current and emerging issues, *Atmos. Chem. Phys.*, 2009, **9**, 5155–5236.
- S. Slikboer, L. Grandy, S. L. Blair, S. A. Nizkorodov, R. W. Smith and H. A. Al-Abadleh, Formation of Light Absorbing Soluble Secondary Organics and Insoluble Polymeric Particles from the Dark Reaction of Catechol and Guaiacol with Fe(III), *Environ. Sci. Technol.*, 2015, **49**, 7793–7801.
- A. Al Nimer, L. Rocha, M. A. Rahman, S. A. Nizkorodov and H. A. Al-Abadleh, Effect of Oxalate and Sulfate on Iron-Catalyzed Secondary Brown Carbon Formation, *Environ. Sci. Technol.*, 2019, **53**, 6708–6717.
- A. Lavi, P. Lin, B. Bhaduri, R. Carmieli, A. Laskin and Y. Rudich, Characterization of Light-Absorbing Oligomers from Phenolic Compounds and Fe(III), *ACS Earth Space Chem.*, 2017, **1**, 637–646.
- J. Y. Ling, F. Sheng, Y. Wang, A. P. Peng, X. Jin and C. Gu, Formation of brown carbon on Fe-bearing clay from volatile phenol under simulated atmospheric conditions, *Atmos. Environ.*, 2020, **228**, 117427.
- H. W. Pang, Q. Zhang, H. L. Wang, D. M. Cai, Y. G. Ma, L. Li, K. N. Li, X. H. Lu, H. Chen, X. Yang and J. M. Chen, Photochemical Aging of Guaiacol by Fe(III)-Oxalate Complexes in Atmospheric Aqueous Phase, *Environ. Sci. Technol.*, 2019, **53**, 127–136.
- A. Laskin, J. Laskin and S. A. Nizkorodov, Chemistry of Atmospheric Brown Carbon, *Chem. Rev.*, 2015, **115**, 4335–4382.
- M. O. Andreae and A. Gelencser, Black carbon or brown carbon? The nature of light-absorbing carbonaceous aerosols, *Atmos. Chem. Phys.*, 2006, **6**, 3131–3148.
- P. Veres, J. M. Roberts, I. R. Burling, C. Warneke, J. de Gouw and R. J. Yokelson, Measurements of gas-phase inorganic and organic acids from biomass fires by negative-ion proton-transfer chemical-ionization mass spectrometry, *J. Geophys. Res. Atmos.*, 2010, **115**, D23302.
- L. E. Hatch, A. Rivas-Ubach, C. N. Jen, M. Lipton, A. H. Goldstein and K. C. Barsanti, Measurements of I/SVOCs in biomass-burning smoke using solid-phase extraction disks and two-dimensional gas chromatography, *Atmos. Chem. Phys.*, 2018, **18**, 17801–17817.
- H. A. Al-Abadleh, Review of the bulk and surface chemistry of iron in atmospherically relevant systems containing humic-like substances, *RSC Adv.*, 2015, **5**, 45785–45811.
- C. R. Usher, A. E. Michel and V. H. Grassian, Reactions on mineral dust, *Chem. Rev.*, 2003, **103**, 4883–4939.
- S. R. Taylor, Abundance of chemical elements in the continental crust: a new table, *Geochim. Cosmochim. Acta*, 1964, **28**, 1273–1285.
- P. N. Sedwick, E. R. Sholkovitz and T. M. Church, Impact of anthropogenic combustion emissions on the fractional solubility of aerosol iron: Evidence from the Sargasso Sea, *Geochem., Geophys., Geosyst.*, 2007, **8**, Q10Q06.
- H. Chen, A. Laskin, J. Baltrusaitis, C. A. Gorski, M. M. Scherer and V. H. Grassian, Coal Fly Ash as a Source of Iron in Atmospheric Dust, *Environ. Sci. Technol.*, 2012, **46**, 2112–2120.
- C. Guieu, S. Bonnet, T. Wagener and M. D. Loye-Pilot, Biomass burning as a source of dissolved iron to the open ocean?, *Geophys. Res. Lett.*, 2005, **32**, L19608.
- A. Ito, S. Myriokefalitakis, M. Kanakidou, N. M. Mahowald, R. A. Scanza, D. S. Hamilton, A. R. Baker, T. Jickells, M. Sarin, S. Bikkina, Y. Gao, R. U. Shelley, C. S. Buck, W. M. Landing, A. R. Bowie, M. M. G. Perron, C. Guieu, N. Meskhidze, M. S. Johnson, Y. Feng, J. F. Kok, A. Nenes and R. A. Duce, Pyrogenic iron: The missing link to high iron solubility in aerosols, *Sci. Adv.*, 2019, **5**, eaau7671.
- R. M. Harrison, A. M. Jones, J. Gietl, J. X. Yin and D. C. Green, Estimation of the Contributions of Brake Dust, Tire Wear, and Resuspension to Nonexhaust Traffic Particles Derived from Atmospheric Measurements, *Environ. Sci. Technol.*, 2012, **46**, 6523–6529.
- A. Salam, M. Hasan, B. A. Begum, M. Begum and S. K. Biswas, Chemical characterization of biomass burning deposits from cooking stoves in Bangladesh, *Biomass Bioenergy*, 2013, **52**, 122–130.
- D. W. Griffin, C. A. Kellogg and E. A. Shinn, Dust in the Wind: Long Range Transport of Dust in the Atmosphere and Its Implications for Global Public and Ecosystem Health, *Global Change and Human Health*, 2001, **2**, 20–33.
- V. Ramanathan, P. J. Crutzen, J. Lelieveld, A. P. Mitra, D. Althausen, J. Anderson, M. O. Andreae, W. Cantrell, G. R. Cass, C. E. Chung, A. D. Clarke, J. A. Coakley, W. D. Collins, W. C. Conant, F. Dulac, J. Heintzenberg, A. J. Heymsfield, B. Holben, S. Howell, J. Hudson, A. Jayaraman, J. T. Kiehl, T. N. Krishnamurti, D. Lubin, G. McFarquhar, T. Novakov, J. A. Ogren, I. A. Podgorny, K. Prather, K. Priestley, J. M. Prospero, P. K. Quinn, K. Rajeev, P. Rasch, S. Rupert, R. Sadourny, S. K. Satheesh, G. E. Shaw, P. Sheridan and F. P. J. Valero, Indian ocean experiment: An integrated analysis of the climate forcing and effects of the great Indo-Asian haze, *J. Geophys. Res. Atmos.*, 2001, **106**, 28371–28398.
- J. Lelieveld, P. J. Crutzen, V. Ramanathan, M. O. Andreae, C. A. M. Brenninkmeijer, T. Campos, G. R. Cass, R. R. Dickerson, H. Fischer, J. A. de Gouw, A. Hansel, A. Jefferson, D. Kley, A. T. J. de Laat, S. Lal, M. G. Lawrence, J. M. Lobert, O. L. Mayol-Bracero, A. P. Mitra, T. Novakov, S. J. Oltmans, K. A. Prather, T. Reiner, H. Rodhe, H. A. Scheeren, D. Sikka and J. Williams, The Indian Ocean experiment: widespread air pollution from South and Southeast Asia, *Science*, 2001, **291**, 1031–1036.



- 23 P. Salgado, D. Contreras, H. D. Mansilla, K. Marquez, G. Vidal, C. J. Cobos and D. O. Martire, Experimental and computational investigation of the substituent effects on the reduction of Fe³⁺ by 1,2-dihydroxybenzenes, *New J. Chem.*, 2017, **41**, 12685–12693.
- 24 S. Hwang, C. H. Lee and I. S. Ahn, Product identification of guaiacol oxidation catalyzed by manganese peroxidase, *J. Ind. Eng. Chem.*, 2008, **14**, 487–492.
- 25 R. L. Crawford, L. E. Robinson and R. D. Foster, Polyguaiacol: a Useful Model Polymer for Lignin Biodegradation Research, *Appl. Environ. Microbiol.*, 1981, **41**, 1112–1116.
- 26 V. M. Nurchi, T. Pivetta, J. I. Lachowicz and G. Crisponi, Effect of substituents on complex stability aimed at designing new iron(III) and aluminum(III) chelators, *J. Inorg. Biochem.*, 2009, **103**, 227–236.
- 27 J. P. Cornard, Rasmiwetti and J. C. Merlin, Molecular structure and spectroscopic properties of 4-nitrocatechol at different pH: UV-visible, Raman, DFT and TD-DFT calculations, *Chem. Phys.*, 2005, **309**, 239–249.
- 28 C. J. Hennigan, J. Izumi, A. P. Sullivan, R. J. Weber and A. Nenes, A critical evaluation of proxy methods used to estimate the acidity of atmospheric particles, *Atmos. Chem. Phys.*, 2015, **15**, 2775–2790.
- 29 F. Wu and N. S. Deng, Photochemistry of hydrolytic iron (III) species and photoinduced degradation of organic compounds. A minireview, *Chemosphere*, 2000, **41**, 1137–1147.
- 30 L. Deguillaume, M. Leriche, K. Desboeufs, G. Mailhot, C. George and N. Chaumerliac, Transition metals in atmospheric liquid phases: Sources, reactivity, and sensitive parameters, *Chem. Rev.*, 2005, **105**, 3388–3431.
- 31 E. A. Pillar, R. X. Zhou and M. I. Guzman, Heterogeneous Oxidation of Catechol, *J. Phys. Chem. A*, 2015, **119**, 10349–10359.
- 32 R. Sander, *NIST Chemistry WebBook, NIST Standard Reference Database Number 69, Henry's Law Constants*, ed. P. J. L. a. W. G. Mallard, National Institute of Standards and Technology, 2018, DOI: 10.18434/T4D303.
- 33 R. A. Washenfelder, A. R. Attwood, C. A. Brock, H. Guo, L. Xu, R. J. Weber, N. L. Ng, H. M. Allen, B. R. Ayres, K. Baumann, R. C. Cohen, D. C. Draper, K. C. Duffey, E. Edgerton, J. L. Fry, W. W. Hu, J. L. Jimenez, B. B. Palm, P. Romer, E. A. Stone, P. J. Wooldridge and S. S. Brown, Biomass burning dominates brown carbon absorption in the rural southeastern United States, *Geophys. Res. Lett.*, 2015, **42**, 653–664.
- 34 G. Albarran, W. Boggess, V. Rassolov and R. H. Schuler, Absorption Spectrum, Mass Spectrometric Properties, and Electronic Structure of 1,2-Benzoquinone, *J. Phys. Chem. A*, 2010, **114**, 7470–7478.
- 35 R. A. Larson and J. M. Hufnal, Oxidative polymerization of dissolved phenols by soluble and insoluble inorganic species, *Limnol. Oceanogr.*, 1980, **25**, 505–512.
- 36 A. Tran, G. Williams, S. Younus, N. N. Ali, S. L. Blair, S. A. Nizkorodov and H. A. Al-Abadleh, Efficient Formation of Light-Absorbing Polymeric Nanoparticles from the Reaction of Soluble Fe(III) with C4 and C6 Dicarboxylic Acids, *Environ. Sci. Technol.*, 2017, **51**, 9700–9708.
- 37 H. Broumand and J. H. Smith, composition of the complexes of iron (III) with phenols and enols, *J. Am. Chem. Soc.*, 1952, **74**, 1013–1016.
- 38 S. Dubey, D. Singh and R. A. Misra, Enzymatic synthesis and various properties of poly(catechol), *Enzyme Microb. Technol.*, 1998, **23**, 432–437.
- 39 C. K. Duesterberg and T. D. Waite, Kinetic modeling of the oxidation of p-hydroxybenzoic acid by Fenton's reagent: Implications of the role of quinones in the redox cycling of iron, *Environ. Sci. Technol.*, 2007, **41**, 4103–4110.
- 40 H. I. Abrash, D. Shih, W. Elias and F. Malekmehr, A Kinetic Study Of The Air Oxidation Of Pyrogallol And Purpurogallin, *Int. J. Chem. Kinet.*, 1989, **21**, 465–476.
- 41 A. Critchlow, R. D. Haworth and P. L. Pauson, Purpurogallin 6 Mechanism of the oxidation of pyrogallol, *J. Chem. Soc.*, 1951, 1318–1325.
- 42 A. Critchlow, E. Haslam, R. D. Haworth, P. B. Tinker and N. M. Waldron, Oxidation of some pyrogallol and purpurogallin derivatives, *Tetrahedron*, 1967, **23**, 2829.
- 43 A. Bach, Purpurogallin-recovery in the oxidation of pyrogallol by means of peroxidase and hydroperoxide, *Ber. Dtsch. Chem. Ges.*, 1914, **47**, 2125–2126.
- 44 M. A. J. Harrison, S. Barra, D. Borghesi, D. Vione, C. Arsene and R. L. Olariu, Nitrated phenols in the atmosphere: a review, *Atmos. Environ.*, 2005, **39**, 231–248.
- 45 Y. Iinuma, O. Boge, R. Grafe and H. Herrmann, Methyl-Nitrocatechols: Atmospheric Tracer Compounds for Biomass Burning Secondary Organic Aerosols, *Environ. Sci. Technol.*, 2010, **44**, 8453–8459.
- 46 C. L. Li, Q. F. He, J. Schade, J. Passig, R. Zimmermann, D. Meidan, A. Laskin and Y. Rudich, Dynamic changes in optical and chemical properties of tar ball aerosols by atmospheric photochemical aging, *Atmos. Chem. Phys.*, 2019, **19**, 139–163.
- 47 H. Li, H. Y. Guo, B. Pan, S. H. Liao, D. Zhang, X. K. Yang, C. G. Min and B. S. Xing, Catechol degradation on hematite/silica-gas interface as affected by gas composition and the formation of environmentally persistent free radicals, *Sci. Rep.*, 2016, **6**, 24494.
- 48 S. W. C. Chien, H. L. Chen, M. C. Wang and K. Sessaiah, Oxidative degradation and associated mineralization of catechol, hydroquinone and resorcinol catalyzed by birnessite, *Chemosphere*, 2009, **74**, 1125–1133.
- 49 D. E. Romonosky, Y. Li, M. Shiraiwa, A. Laskin, J. Laskin and S. A. Nizkorodov, Aqueous Photochemistry of Secondary Organic Aerosol of alpha-Pinene and alpha-Humulene Oxidized with Ozone, Hydroxyl Radical, and Nitrate Radical, *J. Phys. Chem. A*, 2017, **121**, 1298–1309.
- 50 D. E. Romonosky, A. Laskin, J. Laskin and S. A. Nizkorodov, High-Resolution Mass Spectrometry and Molecular Characterization of Aqueous Photochemistry Products of Common Types of Secondary Organic Aerosols, *J. Phys. Chem. A*, 2015, **119**, 2594–2606.
- 51 A. P. Bateman, S. A. Nizkorodov, J. Laskin and A. Laskin, Photolytic processing of secondary organic aerosols



- dissolved in cloud droplets, *Phys. Chem. Chem. Phys.*, 2011, **13**, 12199–12212.
- 52 R. F. Hems and J. P. D. Abbatt, Aqueous Phase Photo-oxidation of Brown Carbon Nitrophenols: Reaction Kinetics, Mechanism, and Evolution of Light Absorption, *ACS Earth Space Chem.*, 2018, **2**, 225–234.
- 53 R. F. Hems, J. S. Hsieh, M. A. Slodki, S. M. Zhou and J. P. D. Abbatt, Suppression of OH Generation from the Photo-Fenton Reaction in the Presence of alpha-Pinene Secondary Organic Aerosol Material, *Environ. Sci. Technol. Lett.*, 2017, **4**, 439–443.
- 54 B. J. Holmes and G. A. Petrucci, Oligomerization of levoglucosan by Fenton chemistry in proxies of biomass burning aerosols, *J. Atmos. Chem.*, 2007, **58**, 151–166.
- 55 A. M'Hemdi, B. Dbira, R. Abdelhedi, E. Brillas and S. Ammar, Mineralization of Catechol by Fenton and Photo-Fenton Processes, *Clean: Soil, Air, Water*, 2012, **40**, 878–885.
- 56 T. B. Nguyen, M. M. Coggon, R. C. Flagan and J. H. Seinfeld, Reactive Uptake and Photo-Fenton Oxidation of Glycolaldehyde in Aerosol Liquid Water, *Environ. Sci. Technol.*, 2013, **47**, 4307–4316.
- 57 J. Rodriguez, D. Contreras, C. Oviedo, J. Freer and J. Baeza, Degradation of recalcitrant compounds by catechol-driven Fenton reaction, *Water Science and Technology*, 2004, **49**, 81–84.

